Materials Advances

ROYAL SOCIETY OF CHEMISTRY

PAPER

View Article Online
View Journal | View Issue

Cite this: *Mater. Adv.*, 2022, 3, 2591

Strong and pure red-emitting Eu^{3+}-doped phosphor with excellent thermal stability for warm WLEDs†

Liang Zhang,[ab] Yonghui Xu,[ab] Xiudi Wu,[ab] Shuwen Yin[a] and Hongpeng You *[abc]

Received 22nd December 2021,
Accepted 28th January 2022

DOI: 10.1039/d1ma01221e

rsc.li/materials-advances

Red-emitting phosphor, as an indispensable part of high-quality white-light-emitting diodes (WLEDs), has received extensive research attention. A red-emitting Eu^{3+}-doped $LiYO_2$ phosphor with excellent luminescence properties was prepared by solid phase reaction. Under the optimal excitation of 395 nm, the specimens displayed strong and pure red emission, the optimal doping concentration and color purity were 0.20 and as high as 98.9%, and the dipole–dipole interaction was found to be responsible for concentration quenching. According to crystallographic structure and Judd–Ofelt theory analysis, the Eu^{3+} ions were located at a low symmetry site, thereby obtaining a high bright red emission. Furthermore, the obtained $LiYO_2$:0.20Eu^{3+} sample possesses outstanding emission thermal stability. Finally, a packaged WLED device based on a $LiYO_2$:0.20Eu^{3+} phosphor with excellent performance was obtained. These results indicate that the as-prepared phosphor has potential for high-quality lighting applications.

Introduction

Today, the world energy shortage has become increasingly serious, and improving energy efficiency is an important approach to effectively relieve the situation.[1] Compared with traditional light sources, phosphor-converted white light-emitting diodes (pc-WLEDs) have higher energy conversion efficiency, long lifetime, are environmentally benign, portable and fast switching, *etc.*[2–5] Conversely, three monochromatic LEDs that realize a white light source, have disadvantages of high cost, different aging properties, complicated circuits, and so on.[6] Therefore, white light from LED-excited phosphors are more promising. Presently, the frequently used methods to produce high-quality white light are blue LED chip excited yellow-emitting (YAG:Ce^{3+}) phosphor, blue LED chip combined with green and red phosphors and near-ultraviolet (n-UV) chip blended with trichromatic phosphors.[7] The former can cause a relatively poor color rendering index (CRI, Ra $<$ 80) due to the insufficient red component of the single yellow phosphor.[8] Hence, the red-emitting phosphor is indispensable for realizing high-quality general lighting. Currently, the main promising red phosphors are nitrides or fluorides. However, nitrides suffer from hash preparation conditions and high cost of raw materials; fluorides are poorly stable and are harmful raw materials.[9,10] These disadvantages restrict their application. Hence, highly effective red phosphors with mild preparation conditions and excellent luminescence properties are in high demand.

In general, the trivalent rare earth europium ion (Eu^{3+}) has received great attention due to its narrow and strong pure red emission, resulting from $^5D_0 \rightarrow {}^7F_J$ (J = 0, 1, 2, 3, 4) transitions.[11–13] Among these transitions, the electric-dipole (ED) transition $^5D_0 \rightarrow {}^7F_0$ can be seen at C_s, C_n, and C_{nv} symmetry. The $^5D_0 \rightarrow {}^7F_1$ and $^5D_0 \rightarrow {}^7F_2$ transitions, as the predominant transitions in most Eu^{3+}-doped phosphor materials, are magnetic-dipole (MD) and hypersensitive ED transitions, respectively. The former intensity is almost irrelevant to the local environment of the Eu^{3+} ion, whereas the latter is greatly dependent on the ligand properties and local symmetry of the Eu^{3+} ion. The $^5D_0 \rightarrow {}^7F_3$ and $^5D_0 \rightarrow {}^7F_4$ transitions are forbidden transitions and dependent on the environment.[14,15] However, the excitation spectrum of a common Eu^{3+}-doped sample is broad, and a strong charge-transfer band is located in the UV region, which is difficult to use in commercial n-UV or blue LED chips. Recently, there have been some reports that Eu^{3+}excitation has an abnormally weak charge transfer band, such as in Sr_2LaNbO_6:Eu^{3+}, $Cs_3GdGe_3O_9$:Eu^{3+}, $LaSc_3(BO_3)_4$:Eu^{3+}, $Ca_2Ga_2SiO_7$:Eu^{3+}, and $Ca_{19}Mg_2(PO_4)_{14}$:Eu^{3+}.[16–20] Hence, a suitable host may lead to a stronger intra-4f transition absorption that matches well with the emission of n-UV or blue LED chips.

[a] *State Key Laboratory of Rare Earth Resource Utilization, Changchun Institute of Applied Chemistry, Chinese Academy of Sciences, Changchun 130022, P. R. China. E-mail: hpyou@ciac.ac.cn; Fax: +86 431 85698041*
[b] *University of Science and Technology of China, Hefei 230026, P. R. China*
[c] *Ganjiang Innovation Academy, Chinese Academy of Sciences, Ganzhou 341000, China*

† Electronic supplementary information (ESI) available See DOI: 10.1039/d1ma01221e

In this paper, we prepare a Eu^{3+}-doped $LiYO_2$ phosphor by the traditional high-temperature solid-phase method. Although $LiYO_2$:Eu^{3+} has been reported before, only a brief study has been done.[21] We prepared this material under different synthesis conditions and systematically studied and analyzed the phase purity and crystal structure. The excitation and emission spectra demonstrate excellent optical properties that contain strong and pure red emission and appropriate excitation, matching well with the LED chip. Furthermore, the relationship between the Eu^{3+}-local environments and spectra is also explored by the Judd–Ofelt theory. The luminescence thermal stability of the sample was investigated by temperature-dependent spectra. Finally, a warm white light LED device is obtained with low correlated color temperature (CCT) and high CRI. These results illustrate that this specimen is an excellent red phosphor for potential application in WLEDs.

Experimental section

$LiY_{1-x}O_2$:xEu^{3+} (x = 0.15, 0.20, 0.25, 0.30, 0.35, 0.40, 0.45, abbreviated as LY:xEu^{3+}) phosphors were prepared by a solid-phase approach. The raw materials containing Li_2CO_3 (99.99%), Y_2O_3 (99.99%) and Eu_2O_3 (99.99%) were weighed stoichiometrically and then poured into a grinding bowl and ground for 20 minutes. The obtained mixture was put into corundum crucibles and heated at 1273 K for 4 h. Finally, the products were furnace-cooled to room temperature and crushed to an even powder for further characterization.

The phase purity of all specimens was obtained by X-ray diffraction (XRD) using a broker AXs D8 diffractometer (40 Kv × 40 mA, Cu-Kα, λ = 0.15405 nm). The morphologies and elemental mappings of the samples were identified by scanning electron microscopy (SEM, Hitachi S-4800) equipped with an energy dispersive spectrometer (EDS). The photoluminescence excitation (PLE) and photoluminescence (PL) spectra were recorded using a high-resolution spectrofluorometer (Edinburgh FLSP-920) equipped with a 450 W xenon lamp. The fluorescence decay curves were obtained from a Lecroy Wave Runner 6100 Digital Oscilloscope (1 GHz) using a tunable laser (pulse with = 4 ns, gate = 50 ns) as the excitation source (Continuum Sunlite OPO). Temperature-dependent PL spectra from 298 to 473 K were collected by Edinburgh Instruments FLSP-920 with a temperature controller.

Results and discussion

Fig. 1a shows the XRD patterns of the representative LY:xEu^{3+} samples and corresponding standard diffraction file card (PDF No. 97-004-5511). All the diffraction peaks of these samples are in agreement with the standard data, demonstrating that the obtained samples are pure phase. Fig. 1b displays the simplified crystal structure of the $LiYO_2$ host. The host lattice contains a distorted YO_6 octahedron in C_1 site symmetry with corresponding bond lengths of 2.36547 (Y–O1), 2.22385 (Y–O1), 2.23650 (Y–O1), 2.22946 (Y–O2), 2.22966 (Y–O2) and 2.40068 (Y–O2) and a LiO_4 polyhedron, and is a monoclinic crystal system with space group $P2_1/c$.[22] According to the valence state and ionic radius, Eu^{3+} (R^{3+}_{Eu} = 0.0947 nm, CN (coordination number) = 6) ions should enter the Y (R^{3+}_{Y} = 0.09 nm, CN = 6) site instead of the Li (R^{+}_{Li} = 0.059 nm, CN = 4) site.[23]

The corresponding refined results of the LY:xEu^{3+} (x = 0.20, 0.25, 0.30, 0.35, 0.40) specimens, using the structure data of $LiYO_2$ (ICSD No. 45511) as the starting model, are shown in Fig. 2a and Fig. S1 (ESI†). The detailed results are listed in Tables S2 and S3 (ESI†), which demonstrate that all results are reliable and rational. Fig. 2b plots the refined cell volume (V) and parameters (a, b, c) of the corresponding samples. It could be found that a, c and V are almost linearly elevated, but b decreases as the Eu^{3+}-concentration increases. According to the previous reports, the decrease in parameter b may be relevant to the special rotation of polyhedra, and there is a sufficiently large (Y/Eu)–O–(Y/Eu) angle in the host. The introduction of larger Eu^{3+} ions increases the bond length and causes a decrease in the (Y/Eu)–O–(Y/Eu) angle.[24,25] Hence, the distance (Y/Eu)–(Y/Eu) and parameter b, decrease.

Fig. 3a displays the excitation (λ_{em} = 613 nm) and emission (λ_{ex} = 395 nm) spectra of LY:0.20Eu^{3+}. The PLE spectrum covering 200 to 550 nm comprises a relatively weak broad band ranging from 230 to 280 nm and a series of characteristic 4f–4f line bands; the peak values are 270, 307, 323, 364, 382, 395, 417, 468, 527, and 539 nm. These bands result from the charge transfer band, $^7F_0 \rightarrow {}^5H_6$, $^7F_0 \rightarrow {}^5H_3$, $^7F_0 \rightarrow {}^5D_4$, $^7F_0 \rightarrow {}^5G_2$,

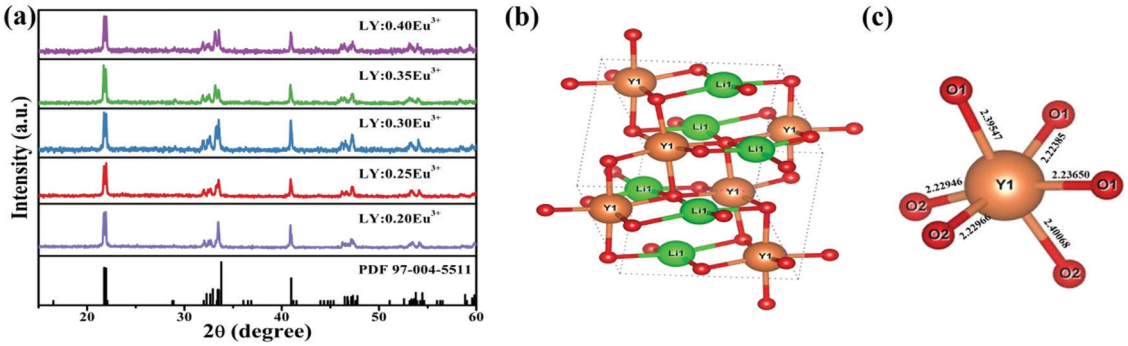

Fig. 1 (a) XRD patterns of $LiYO_2$:xEu^{3+} (x = 0.20–0.40) and the standard XRD card (PDF No. 97-004-5511). (b) The unit cell structure of $LiYO_2$ and (c) the bond lengths of the InO_6 octahedra.

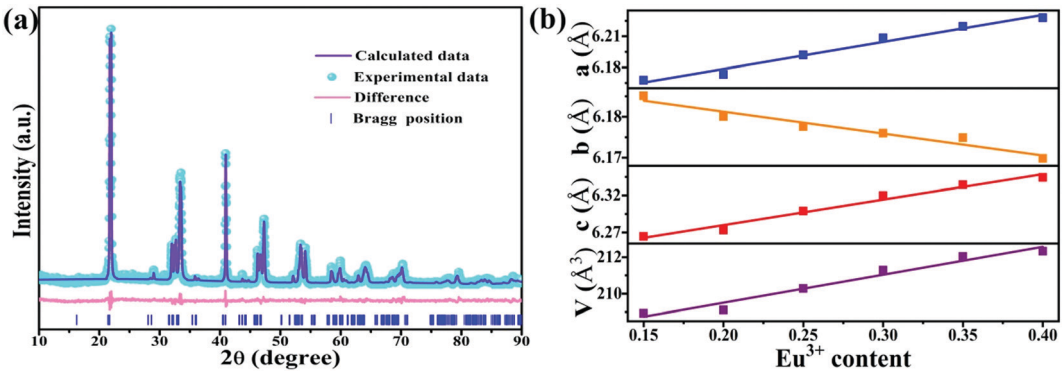

Fig. 2 (a) The Rietveld refinements of $LiYO_2$:0.20Eu^{3+} and (b) the relationship between lattice parameters and the differing amounts of Eu^{3+} in the $LiYO_2$ host.

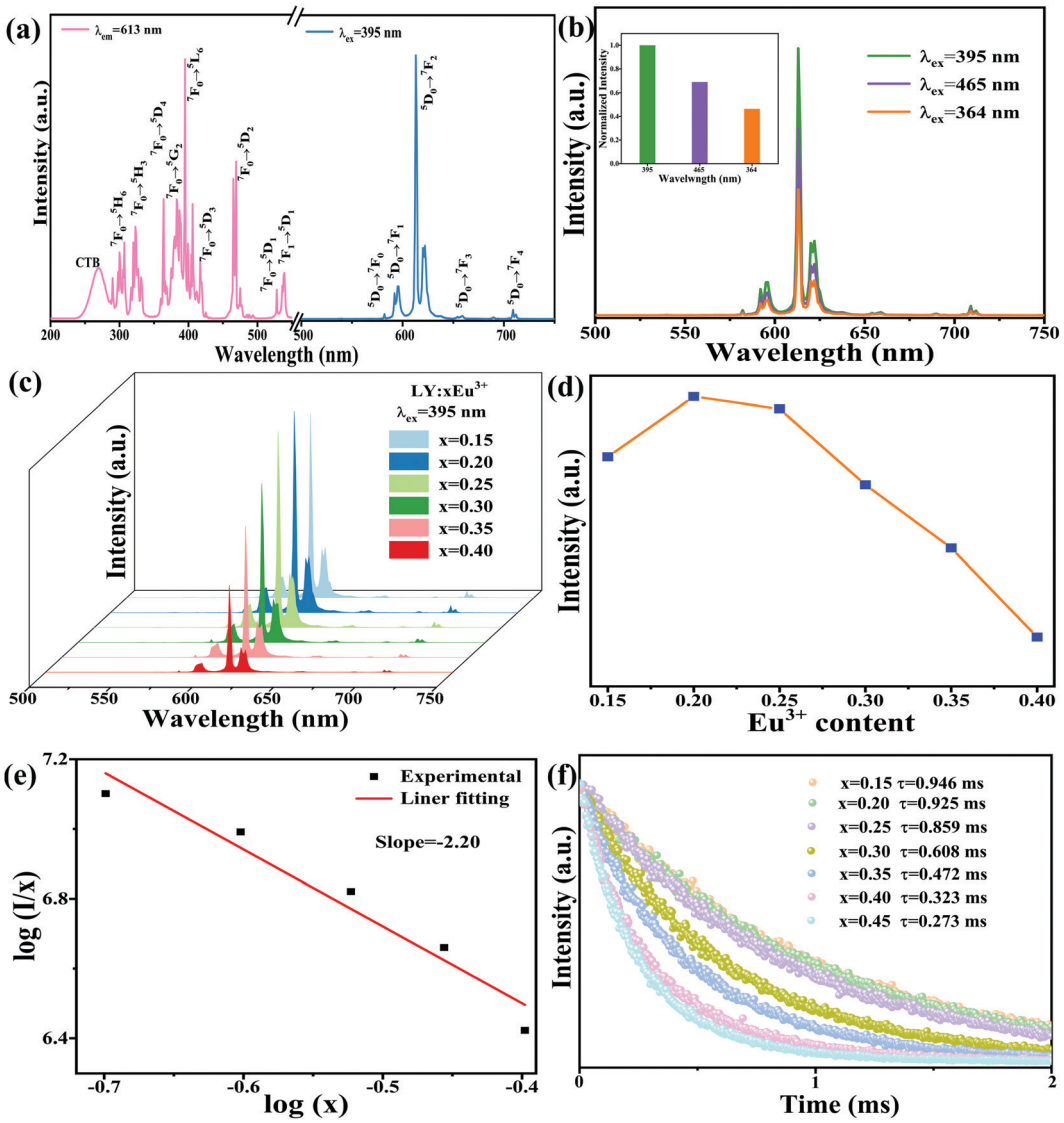

Fig. 3 (a) and (b) Excitation and emission spectra with different excitation wavelengths of $LiYO_2$:0.20Eu^{3+}. (c) Emission spectra for different concentrations of Eu^{3+} and (d) relative intensity of the $LiYO_2$:xEu^{3+} samples. (e) Dependence of log(I/x) with log x. (f) The PL decay curves of $LiYO_2$:xEu^{3+}.

$^7F_0 \rightarrow {}^5L_6$, $^7F_0 \rightarrow {}^5D_3$, $^7F_0 \rightarrow {}^5D_2$, $^7F_0 \rightarrow {}^5D_1$, and $^7F_1 \rightarrow {}^5D_1$ transitions of the Eu^{3+} ions, respectively.[26] Under 395 nm light irradiation, the emission spectrum displays some distinct transition bands belonging to the $^5D_0 \rightarrow {}^7F_J$ (J = 0, 1, 2, 3, 4) transitions of the Eu^{3+} ions with centers of 582, 595, 613, 658, and 709 nm.[27] It is important to note that the excitation peak at 395 nm has maximum absorption and produces the strongest luminescence in comparison with the other excitations, as seen in Fig. 3b. Hence, the emission spectra of LY:xEu^{3+} samples with different Eu^{3+}-content were recorded upon excitation with 395 nm light, as shown in Fig. 3c and d. When the Eu^{3+}-concentration increases, the PL intensity presents a trend of increasing at first and then decreasing, and the optimum doped concentration is 0.20. The phenomenon of the decrease in PL intensity is caused by concentration quenching due to the existence of energy transfer between adjacent ions. Moreover, the mechanism of concentration quenching mainly includes electric multipolar and exchange interactions. The quenching mechanism can be further distinguished by the critical distance (Rc) obtained by the following expression.[28,29]

$$\mathrm{Rc} = 2\left(\frac{3V}{4\pi x_c N}\right)^{1/3} \quad (1)$$

where V, x_c and N are the volume of the crystal unit cell, doped ions of the critical concentration and the number of sites that could be occupied by doped ions, respectively. V, x_c and N are 209.111 Å^3, 0.20 and 4 in the Eu^{3+}-doped $LiYO_2$ phosphors. According to expression (1), the value of Rc is 7.93 (>5 Å), demonstrating that the quenching mechanism is dominated by the electric multipolar interaction. Correspondingly, the electric multipolar interaction is classified as dipole–dipole (d–d), dipole–quadrupole (d–q), and quadrupole–quadrupole (q–q) interactions, when the interaction constant θ is 6, 8 and 10, respectively. The value of θ can be found from the slope using the following formula.[30,31]

$$\log\left(\frac{I}{x}\right) = C - \frac{\theta}{3}\log x \quad (2)$$

In which x and I are the concentration of doped ions (≥optimal concentration) and corresponding emission intensity, respectively, and C is the constant. Therein, we get a slope of −2.20 (Fig. 3e). The θ value is 6.60, closer to 6, which further suggests that the mechanism is predominated by d–d interactions.

The Commission Internationale de L'Eclairage (CIE) chromaticity coordinates of a series of $LiYO_2$:xEu^{3+} and their corresponding color purity are shown in Fig. S2 and Table S4 (ESI†). The color purity be expressed as

$$\text{color purity} = \frac{\sqrt{(x-x_i)^2+(y-y_i)^2}}{\sqrt{(x_d-x_i)^2+(y_d-y_i)^2}} \times 100\% \quad (3)$$

where (x_d, y_d) and (x_i, y_i) are the dominant wavelength point and white illuminant point, respectively. (x, y) are the CIE chromaticity coordinates of the sample. For the $LiYO_2$:0.20Eu^{3+}, (x_d, y_d) and (x, y) are (0.665, 0.334) and (0.662, 0.335), respectively, the color purity of $LiYO_2$:0.20Eu^{3+} is as high as 98.9%, and the coordinates are very close to the National Television Standard Commercial red light (0.666, 0.333), indicating that the as-prepared phosphor sample has potential application for WLEDs as a red component.

In order to further confirm the energy transfer, the fluorescence lifetime curves of $LiY_{1-x}O_2$:xEu^{3+} are plotted in Fig. 3f. All the curves are measured at 395 nm excitation and 613 nm emission, and the values of the corresponding lifetimes are estimated as follows.

$$\tau = \frac{\int_0^\infty tI(t)\mathrm{d}t}{\int_0^\infty I(t)\mathrm{d}t} \quad (4)$$

According to eqn (4), the lifetimes of Eu^{3+} are 0.946, 0.925, 0.859, 0.608, 0.472, 0.323, 0.273 ms, at Eu^{3+}-concentrations 0.15, 0.20, 0.25, 0.30, 0.35, 0.40, 0.45, respectively. The lifetime monotonically decreases with increasing Eu^{3+}-content, which is ascribed to the energy transfer among Eu^{3+} ions.

The Judd–Ofelt (J–O) theory is extensively used to understand and characterize the spectral properties of trivalent rare earth ions in hosts. Hence, we employ intensity parameters $\Omega_{2,4}$ based on J–O theory to obtain detailed insight into the relationship between the Eu^{3+} local environments and corresponding spectra.

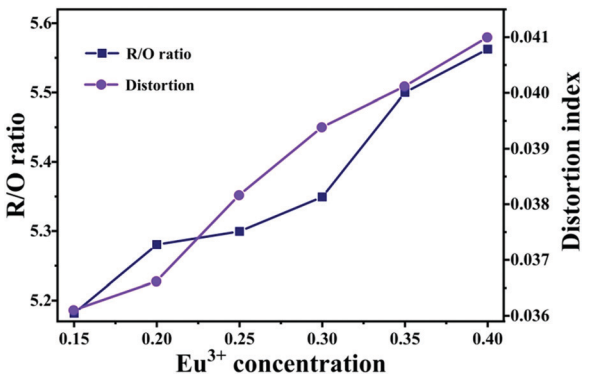

Fig. 4 Calculated R/O values and polyhedral distortion.

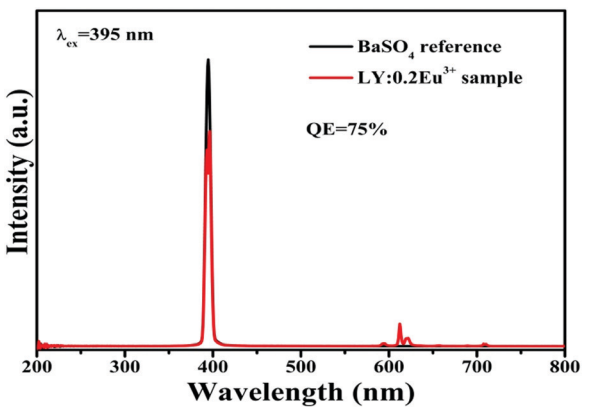

Fig. 5 Quantum efficiency of the LY:0.20Eu^{3+} phosphor.

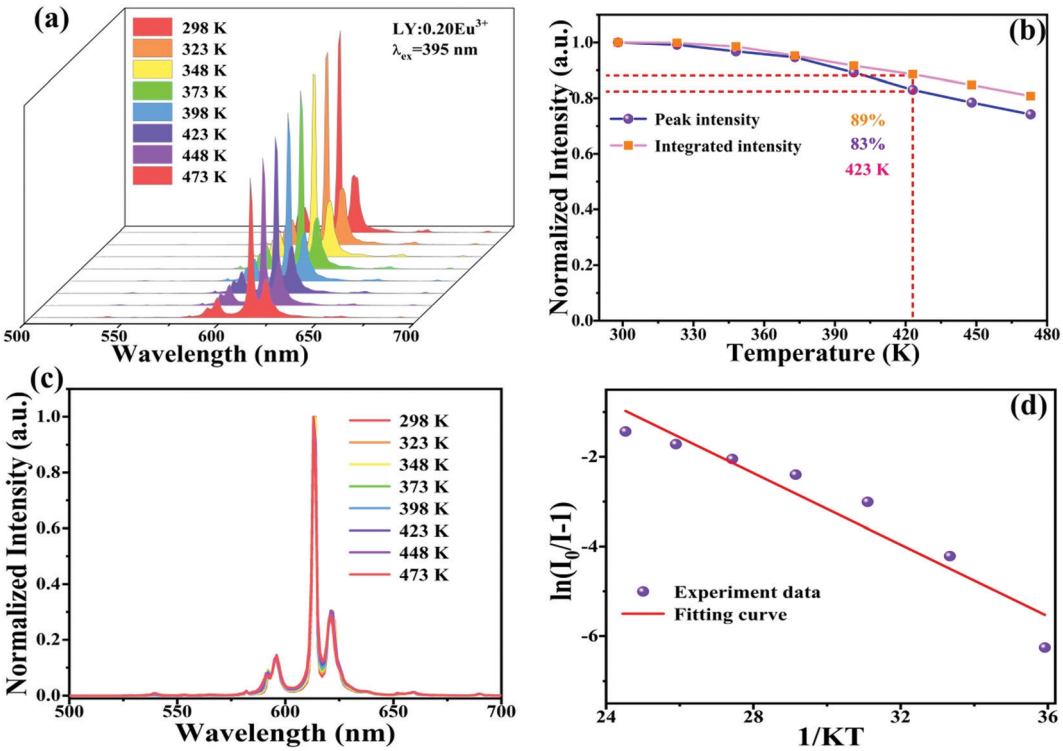

Fig. 6 (a)–(c) PL spectra, the relative peak and integrated intensity, and normalized PL spectra at different temperatures (298–473 K) of the $LiYO_2$:0.20Eu^{3+} sample. (d) The linear relationship of $\ln(I_0/I - 1)$ with $1/KT$.

The intensity parameters of the optimal sample $LiYO_2$:020Eu^{3+} could be estimated by the following expressions.[16,32–34]

$$I = \sum_{J=0,1,2,3,4} I_{^7F_J} = a \sum_{J=0,1,2,3,4} A_{^7F_J} \quad (5)$$

$$\sum_{J=0,1,2,3,4} A_{^7F_J} = \frac{1}{\tau} \quad (6)$$

$$I_{^7F_J} = aA_{^7F_J} \quad (7)$$

$$A^{MD}_{J\to J^\circ} = \frac{64\pi^4\nu^3}{3h(2J+1)} n^3 S_{MD} \quad (8)$$

$$A^{ED}_{J\to J^\circ} = \frac{64\pi^4\nu^3 e^2}{3h(2J+1)} \frac{n(n^2+2)^2}{9} \times \Omega_\lambda \psi J \| U^\lambda \| \psi^\circ J^{\circ 2} \quad (9)$$

where I denotes the total relative integrated intensity (sum of all the $^5D_0 \rightarrow {}^7F_J$ (J = 0, 1, 2, 3, 4) transitions). $I_{^7F_J}$ and $A_{^7F_J}$ are the integrated emission intensity and radiative transition rate (corresponding to $^5D_0 \rightarrow {}^7F_J$ (J = 0, 1, 2, 3, 4) transitions). The ν, $\hbar$, τ, $(2J+1)$, a, e, n and S_{MD} are the center wavenumber for the $J \rightarrow J^\circ$ transition, Planck's constant (6.627×10^{-27}), lifetime (0.925 ms), degeneracy of the initial state, transition constant, elementary charge (4.80×10^{-10}), refractive index and magnetic dipole strength (7.83×10^{-42}), respectively. $\psi J \| U^\lambda \| \psi^\circ J^{\circ 2}$ refers to the reduced matrix element for the $J \rightarrow J^\circ$ electric-dipole transitions, when J° are 2 and 4, corresponding to 0.0032 and 0.0023.[35] For Eu^{3+} ions, the radiative transition rate of the magnetic dipole transition ($^5D_0 \rightarrow {}^7F_1$) is free from a change in the crystal field. Hence, a and n are found to be 0.004856 and 3.435 with the help of eqn (5)–(8). Later, according to eqn (9), Ω_2 and Ω_4 are 5.948×10^{-20} and 5.620×10^{-21}, respectively. Generally, the value of Ω_2 is relevant to the local crystal field environment, whereas Ω_4 is related to the bulk properties and the rigidity of the host lattice. The low symmetry of the Eu^{3+}-coordinated environment will cause a large Ω_2 value, which is consistent with Eu^{3+} ions replacing the Y^{3+} of the low symmetry C_1 site. Moreover, the asymmetric ratios of the R/O ratio (ratio of integrated intensity of $^5D_0 \rightarrow {}^7F_2$ and $^5D_0 \rightarrow {}^7F_1$) are much larger than 1, and the value gradually enlarges with increasing Eu^{3+} concentration (Fig. 4), further demonstrating that the Eu^{3+} ions are located at asymmetric sites.[36] The polyhedral distortion index can be obtained by $D = \frac{1}{n}\sum_{i=1}^{n} \frac{|l_i - l_{av}|}{l_{av}}$.[37] The results indicate that the distortion gradually increases as Eu^{3+} increases. As we know, the larger the distortion is, the lower the symmetry of the site. Hence, the results are consistent with the R/O ratio. These results further demonstrate that the obtained phosphor could provide a high level of bright red emission. In addition, the quantum yields are found to be 75% upon 395 nm excitation for the LY:0.20Eu^{3+} (Fig. 5).

The thermal stability of the phosphor is a vital performance objective in practical applications because the working temperature of LED equipment is unavoidably over 400 K and affects the service life, light output and color rendering index.[35,38] Fig. 6a displays the temperature-dependent

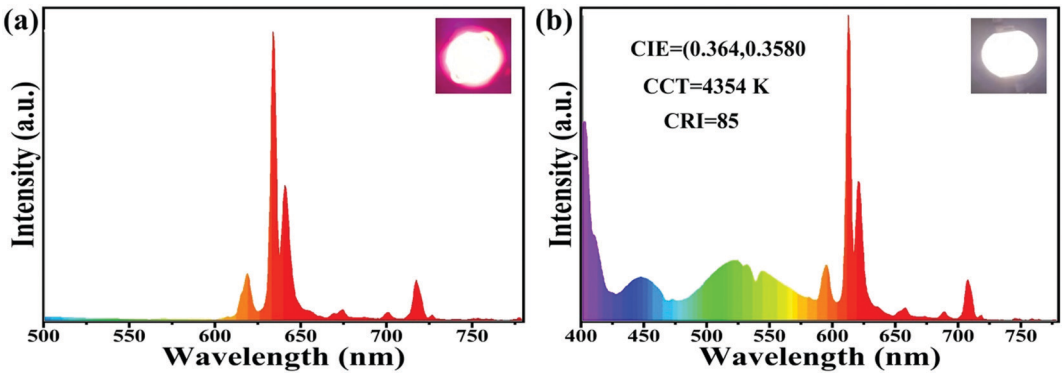

Fig. 7 Electroluminescence spectra and photographs of (a) n-UV LED chip + $LiYO_2$:0.20Eu^{3+} phosphor and (b) n-UV LED chip + $BaMgAl_{10}O_{17}$:Eu^{2+} + $(Sr, Ba)_2SiO_4$:Eu^{2+} + $LiYO_2$:020Eu^{3+}.

(recorded from 298 to 473 K) emission spectra of the optimum $LiYO_2$:020Eu^{3+} sample with 395 nm excitation. Not surprisingly, the luminescence intensity gradually decreases as the temperature increases, which is due to the high working temperature aggravating molecular heat movement and thus enhancing nonradiative transitions. Unexpectedly, the normalized PL peak intensity and integrated emission intensity of the sample still retain 83% and 89% of the starting intensity recorded at 298 K when measured at 473 K (Fig. 6b), respectively, indicating that the $LiYO_2$:020Eu^{3+} phosphor possesses excellent luminescence thermal stability, due to its excellent structural rigidity. From Fig. 6c, we can see that the PL spectrum profiles are almost the same, demonstrating that the phosphor sample has high color stability.

In order to further comprehend the luminescence thermal quenching phenomenon, the activation energy of the $LiYO_2$:020Eu^{3+} specimen could be obtained using the Arrhenius equation.[39]

$$I = \frac{I_0}{1 + C\exp\left(-\frac{Ea}{KT}\right)} \quad (10)$$

I and I_0 represent the emission intensities at $T = T$ and $T =$ 298 K, respectively. C is a constant, and $K = 8.62 \times 10^{-5}$ eV K^{-1}. According to eqn (10), the activation energy (Ea) is found to be 0.399 eV obtained by fitting the $\ln(I_0/I - 1)$ *vs.* $1/kT$ curve, as shown in Fig. 6d. In addition, the emission intensity remained essentially unchanged after the sample was placed in the air for two weeks (Fig. S3, ESI†), demonstrating that the sample has excellent chemical stability. A comparison of some reports of Eu^{3+}-doped phosphors shows that the LY:0.20Eu^{3+} samples have good luminescence properties (Table S5, ESI†).

In view of the excellent luminescence performance, suitable synthetic methods and high thermal stability of the prepared $LiYO_2$:Eu^{3+} red phosphor, a WLED prototype device was assembled based on an n-UV LED chip (395 nm) packed with commercial blue, green and synthesized red phosphors ($BaMgAl_{10}O_{17}$:Eu^{2+} + $(Sr, Ba)_2SiO_4$:Eu^{2+} + $LiYO_2$:020Eu^{3+}) to assess the potential application prospects in the field of lighting. The electroluminescence (EL) spectra and real scene photographs of the as-fabricated pc-LED devices under a current of 20 mA are shown in Fig. 7. The obtained $LiYO_2$:0.20Eu^{3+} phosphor specimen could efficiently convert the light of the n-UV LED chip into highly pure red light. Simultaneously, an LED device with bright warm white light is obtained by blending trichromatic phosphors, and the CIE chromaticity coordinates, CRI and CCT are (0.364, 0.358), 85, and 4354 K, respectively.

Conclusion

To summarise, we synthesized a red Eu^{3+}-doped LiYO2 phosphor and investigated the phase purity, crystal structure, luminescent properties and local environment of Eu^{3+} ions. By irradiating with light at 395 nm, the sample showed a strong red emission, mainly resulting from the $^5D_0 \rightarrow {}^7F_2$ transition, and the color purity is up to 98.9%. The optimal doped concentration and concentration quenching mechanism are 0.20 and d–d interaction, respectively. Meanwhile, by J–O theory, the intensity parameters Ω_2 and Ω_4 of $LiYO_2$:020Eu^{3+} are 5.948×10^{-20} and 5.620×10^{-21}, and the R/O ratio and polyhedral distortion index gradually enhance with increasing Eu^{3+}-content. Additionally, the phosphor sample presented excellent thermal stability with an emission intensity at 423 K, 89% of 398 K. In addition, the activation energy (Ea) is 0.399 eV. The CCT, CRI and CIE chromaticity coordinates of the assembled warm WLED are 4354 K, 85, and (0.364, 0.358), respectively. Hence, the obtained $LiYO_2$:Eu^{3+} can be applied for WLEDs as a promising red-emitting phosphor.

Conflicts of interest

There are no conflicts of interest to declare.

Acknowledgements

This study is financially supported by the National Natural Science Foundation of China (Grant No. 52072363 and 21771175), the Key Research Program of the Chinese Academy of Sciences (Grant No. ZDRW-CN-2021-3), and the Natural Science Foundation of Jilin Province (20200201106JC).

References

1 Z. Xia and Q. Liu, *Prog. Mater. Sci.*, 2016, **84**, 59–117.
2 B. Shao, J. Huo and H. You, *Adv. Opt. Mater.*, 2019, 1900319.
3 F. Hong, H. Xu, G. Pang, G. Liu, X. Dong and W. Yu, *Chem. Eng. J.*, 2020, **390**, 124579.
4 S. Ye, F. Xiao, Y. X. Pan, Y. Y. Ma and Q. Y. Zhang, *Mater. Sci. Eng., R*, 2010, **71**, 1–34.
5 L. Zhang, Y. Xu, S. Yin and H. You, *J. Alloys Compd.*, 2022, **891**, 162042.
6 M. S. Shur and R. Zukauskas, *Proc. IEEE.*, 2005, **93**, 1691–1703.
7 L. Zhang, L. Dong, Y. Xu, S. Yin and H. You, *Dalton Trans.*, 2021, **50**, 1366–1373.
8 F. Hong, H. Cheng, G. Liu, X. Dong, W. Yu and J. Wang, *Inorg. Chem.*, 2018, **57**, 9892–9901.
9 Z. Zhou, N. Zhou, M. Xia, M. Yokoyama and H. T. Hintzen, *J. Mater. Chem. C*, 2016, **4**, 9143–9161.
10 B. Wang, H. Lin, J. Xu, H. Chen and Y. Wang, *ACS Appl. Mater. Interfaces*, 2014, **6**, 22905–22913.
11 Z. Mu, Y. Hu, L. Chen, X. Wang, G. Ju, Z. Yang and R. Chen, *Ceram. Int.*, 2014, **40**, 2575–2579.
12 Z. Mu, Y. Hu, L. Chen and X. Wang, *J. Electrochem. Soc.*, 2011, **158**, J287.
13 M. Liao, Z. Mu, S. Zhang, F. Wu, Z. Nie, Z. Zheng, X. Feng, Q. Zhang, J. Feng and D. Zhu, *J. Lumin.*, 2019, **210**, 202–209.
14 K. Binnemans, *Coord. Chem. Rev.*, 2015, **295**, 1–45.
15 E. Niyama, H. F. Brito, M. Cremona, E. E. S. Teotonio, R. Reyes, G. E. S. Brito and M. C. F. C. Felinto, *Spectrochim. Acta, Part A*, 2005, **61**, 2643–2649.
16 Y. Hua, W. Ran and J. S. Yu, *Chem. Eng. J.*, 2021, **406**, 127154.
17 P. Dang, G. Li, X. Yun, Q. Zhang, D. Liu, H. Lian, M. Shang and J. Lin, *Light: Sci. Appl.*, 2021, **10**, 29.
18 S. Wang, Y. Xu, T. Chen, W. Jiang, J. Liu, X. Zhang, W. Jiang and L. Wang, *Chem. Eng. J.*, 2021, **404**, 125912.
19 G. K. Behrh, R. Gautier, C. Latouche, S. Jobic and H. Serier-Brault, *Inorg. Chem.*, 2016, **55**, 9144–9146.
20 G. Zhu, Z. Ci, Y. Shi, M. Que, Q. Wang and Y. Wang, *J. Mater. Chem. C*, 2013, **1**, 5960–5969.
21 M. D. Faucher, O. K. Moune, M. G. Alves, B. Piriou, P. Sciau and M. Pham-Thi, *J. Solid State Chem.*, 1996, **121**, 457–466.
22 O. Kyoung Moune, J. Dexpert-Ghys, B. Piriou, A. Marie-Gabrielle and M. D. Faucher, *J. Alloys Compd.*, 1998, **275-277**, 258–263.
23 R. Shannon, *Acta Crystallogr., Sect. A*, 1976, **32**, 751–767.
24 L. Yu, H. Yan, Y. Fan, J. Zhang, Z. Ma, W. Zhou, Y. Chen, F. Pan and S. Lian, *J. Mater. Chem. C*, 2018, **6**, 10723–10729.
25 M. Chen, Z. Xia, M. S. Molokeev, C. C. Lin, C. Su, Y.-C. Chuang and Q. Liu, *Chem. Mater.*, 2017, **29**, 7563–7570.
26 A. Tyagi, S. Nigam, V. Sudarsan, C. Majumder, R. K. Vatsa and A. K. Tyagi, *Inorg. Chem.*, 2020, **59**, 12659–12671.
27 J. Huo, A. Yu, Q. Ni, D. Guo, M. Zeng, J. Gao, Y. Zhang and Q. Wang, *Inorg. Chem.*, 2020, **59**, 15514–15525.
28 G. Blasse, *Phys. Lett. A*, 1968, **28**, 444–445.
29 J. Xiang, Z. Zhou, J. Zheng, Y. Chen, H. Suo, X. Zhao, L. Zhao and C. Guo, *Opt. Mater.*, 2020, **109**, 110344.
30 N. Zhang, J. Zheng, J. Gao, Y. Wu, R. Zhang, T. Li and C. Guo, *Dyes Pigm.*, 2017, **136**, 601–611.
31 H. Xiong, Y. Zhang, Y. Liu, T. Gao, L. Zhang, Z.-A. Qiao, L. Zhang, S. Gan and Q. Huo, *J. Alloys Compd.*, 2019, **782**, 845–851.
32 B. Tian, B. Chen, Y. Tian, X. Li, J. Zhang, J. Sun, H. Zhong, L. Cheng, S. Fu, H. Zhong, Y. Wang, X. Zhang, H. Xia and R. Hua, *J. Mater. Chem. C*, 2013, **1**, 2338.
33 G. Bai, M.-K. Tsang and J. Hao, *Adv. Opt. Mater.*, 2015, **3**, 431–462.
34 M. H. V. Werts, R. T. F. Jukes and J. W. Verhoeven, *Phys. Chem. Chem. Phys.*, 2002, **4**, 1542–1548.
35 N. Yang, J. Li, Z. Zhang, D. Wen, Q. Liang, J. Zhou, J. Yan and J. Shi, *Chem. Mater.*, 2020, **32**, 6958–6967.
36 X. Geng, Y. Xie, S. Chen, J. Luo, S. Li, T. Wang, S. Zhao, H. Wang, B. Deng, R. Yu and W. Zhou, *Chem. Eng. J.*, 2021, **410**, 128396.
37 J. Zhang, T. Zhang, Z. Qiu, S. Liu, J. Zhang, W. Zhou, L. Yu and S. Lian, *Inorg. Chem.*, 2018, **57**, 12354–12363.
38 Y. Wei, L. Cao, L. Lv, G. Li, J. Hao, J. Gao, C. Su, C. C. Lin, H. S. Jang, P. Dang and J. Lin, *Chem. Mater.*, 2018, **30**, 2389–2399.
39 D. Zhao, S.-R. Zhang, Y.-P. Fan, B.-Z. Liu, Y.-N. Li, L.-Y. Shi and S.-J. Dai, *ACS Sustainable Chem. Eng.*, 2020, **8**, 18992–19002.